This is the accepted manuscript made available via CHORUS. The article has been published as:

Reversible ratchet effects for vortices in conformal pinning arrays

C. Reichhardt, D. Ray, and C. J. Olson Reichhardt

Phys. Rev. B **91**, 184502 — Published 4 May 2015

DOI: 10.1103/PhysRevB.91.184502

Reversible Ratchet Effects for Vortices in Conformal Pinning Arrays

C. Reichhardt, D. Ray, and C. J. Olson Reichhardt
Theoretical Division, Los Alamos National Laboratory, Los Alamos, New Mexico 87545 USA
(Dated: April 17, 2015)

A conformal transformation of a uniform triangular pinning array produces a structure called a conformal crystal which preserves the six-fold ordering of the original lattice but contains a gradient in the pinning density. Here we use numerical simulations to show that vortices in type-II superconductors driven with an ac drive over gradient pinning arrays produce the most pronounced ratchet effect over a wide range of parameters for a conformal array, while square gradient or random gradient arrays with equivalent pinning densities give reduced ratchet effects. In the conformal array, the larger spacing of the pinning sites in the direction transverse to the ac drive permits easy funneling of interstitial vortices for one driving direction, producing the enhanced ratchet effect. In the square array, the transverse spacing between pinning sites is uniform, giving no asymmetry in the funneling of the vortices as the driving direction switches, while in the random array, there are numerous easy-flow channels present for either direction of drive. We find multiple ratchet reversals in the conformal arrays as a function of vortex density and ac amplitude, and correlate the features with a reversal in the vortex ordering, which is greater for motion in the ratchet direction. The enhanced conformal pinning ratchet effect can also be realized for colloidal particles moving over a conformal array, indicating the general usefulness of conformal structures for controlling the motion of particles.

PACS numbers: 74.25.Wx,74.25.Uv

I. INTRODUCTION

When an assembly of particles are placed in an asymmetric potential, a net dc particle flow can arise due to a ratchet effect that occurs when an ac drive is applied or when the substrate is periodically switched on and off in the presence of a thermal bath[1,2]. Ratchet effects on asymmetric substrates have been extensively studied in colloidal systems[3–5], granular matter[6,7], and polymers[8,9]. Ratchet effects also appear in ac-driven vortices in type-II superconductors in the presence of an asymmetric substrate[10–15], such as a quasi-one-dimensional periodic array produced by asymmetrically modulating the sample thickness[10,16–19], etching funnel-shaped channels for vortex flow[11,20–24], introducing asymmetry to the sample edges[25], or adding periodic pinning arrays in which the individual pinning sites have some form of intrinsic asymmetry[13,14,26–35]. At lower vortex densities when collective interactions between vortices are weak, the ratchet effect produces a dc flow of vortices in the easy flow direction of the asymmetric substrate; however, when collective effects are present it is possible to have reversals of the ratchet effect where for one set of parameters the vortices move in the easy direction while for another set of parameters they move in the hard direction[13–16,18,27–33]. A ratchet effect can also be produced by a pinning array containing symmetric pinning sites arranged with a density gradient. Olson *et al.*[12] first studied vortex ratchet effects for random gradient array pinning geometries and found that the vortices undergo a net dc flow in the easy direction. Experiments and simulations later showed that for a square array of pinning sites with constant pinning density but with a gradient in pinning site size, a variety of forward and reverse vortex ratchet behaviors occur[36]. Experiments on triangular pinning arrays with a density gradient also revealed a forward ratchet effect at low fields with a reversal at higher fields[37,38].

Recently a new type of pinning geometry was proposed that is constructed by conformally transforming a triangular pinning lattice to create what is called a conformal pinning array, abbreviated Conf in this work[39–41]. As in the original triangular lattice, each pinning site in the transformed array has six neighbors separated by 60°; however, the distance to each neighbor is no longer constant, producing a density gradient in the pinning sites[42,43]. In Fig. 1(a) we show a periodic lattice composed of three conformal pinning arrays with the same orientation. Experimental structures with nearly conformal geometries have been observed for magnetically interacting particles subjected to a gravitational force, and due to the arching nature of the conformal array, the magnetic conformal crystals were dubbed gravity's rainbow structures[43]. Similar conformal structures have also been studied in foams[45,46] and in charged particle ordering in confined geometries[46]. In the superconducting system, an arrangement of two Conf arrays placed with their minimum pinning density regions in the center of the sample produces an enhanced critical current or depinning force compared to an equivalent number of pinning sites placed in a uniform periodic, uniform random, or random density gradient array[39]. The enhancement results both from the natural density gradient formed by the vortices as they enter the sample from the edges and form a Bean state, and from the preservation of local six-fold ordering in the Conf array[39,41]. The suppression of easy vortex flow channels which arise in periodic and random arrays by the arching conformal structure also plays a role in the enhancement. Only at the integer matching fields do the periodic pinning arrays produce higher crit-

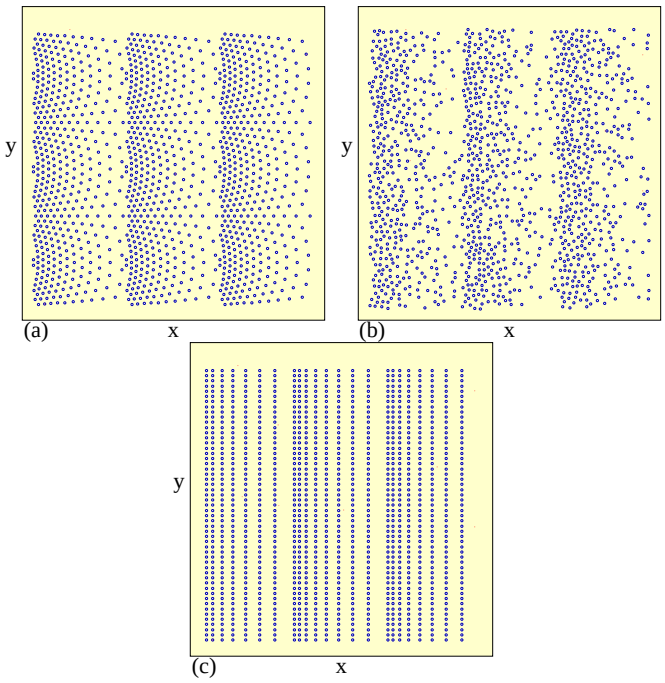

FIG. 1: The system geometry showing the locations of the pinning sites for samples with $n_p = 1.0$. Pinning gradients run along the x direction. (a) Conformal pinning (Conf). (b) Random pinning with a periodic gradient (RandG). (c) Square pinning with a gradient (SquareG). For each sample we apply an ac drive along the x direction and measure the average net vortex displacements $\langle \Delta X \rangle$ in the x direction.

ical currents than the Conf array[41]. Subsequent experimental studies confirmed that the Conf array produces enhanced pinning over a wide range of fields compared to uniform periodic pinning or uniform random pinning arrangements[47,48]. Other experiments have shown enhanced critical currents in systems with periodic arrays when a gradient in the pinning density is introduced[49]. There have also been studies of hyperbolic-tesselation arrays which have a gradient in the pinning density[50].

Since conformal pinning arrays have an intrinsic asymmetry, it is natural to ask whether a ratchet effect can occur under application of an ac drive, and if so, whether this ratchet effect would be enhanced compared to other pinning array geometries with density gradients, or whether ratchet reversals could be possible. In Fig. 1 we illustrate three examples of the gradient pinning array geometries we consider in this work: conformal pinning (Conf) [Fig. 1(a)], random pinning with a gradient (RandG) [Fig. 1(b)], and a square pinning array containing a gradient along the x direction (SquareG) [Fig. 1(c)]. In each case, both the gradient and the applied ac drive are along the x direction, while the easy-flow direction for vortex motion is in the negative x direction. In addition to superconducting vortex realizations of these geometries, similar pinning arrangements could also be created in colloidal systems using optical trap arrays.

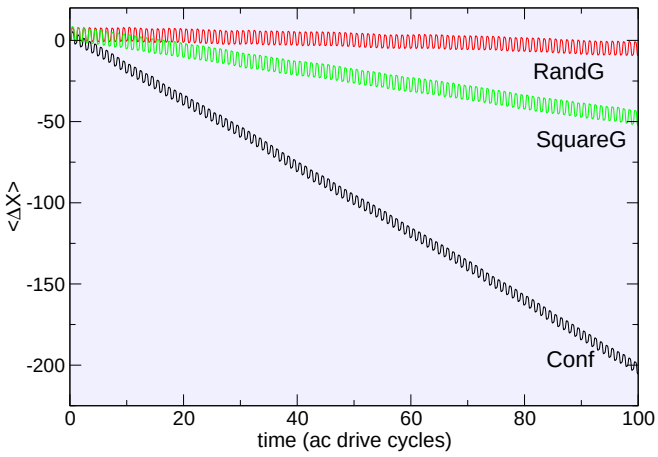

FIG. 2: The average net displacement $\langle \Delta X \rangle$ vs time measured in ac drive cycles for the systems in Fig. 1 at $B/B_\phi = 1.0$, $F_p = 1.0$, and $F_{ac} = 0.55$. Bottom black curve: Conf array; middle green curve: SquareG array; upper red curve: RandG array. Here the Conf array produces a ratchet that is four times more effective than the SquareG array and 20 times more effective than the RandG array.

II. SIMULATION AND SYSTEM

We consider a two-dimensional system with periodic boundary conditions in the x and y directions. The sample size is $L \times L$ with $L = 36\lambda$, where distance is measured in units of the London penetration depth λ. The applied magnetic field is perpendicular to the system in the $\hat{\mathbf{z}}$ direction. Our results apply to the London limit regime in which the vortices can be treated as rigid objects, when the coherence length ξ is much smaller than λ. The pinning sites are modeled as in previous studies of conformal pinning arrays[39–41] by non-overlapping parabolic circular traps with radius R_p and a maximum pinning force of F_p. We place the N_p pinning sites in a conformal array (Conf), as described in previous work[39], in a random arrangement with a gradient (RandG), or in a square array with a density gradient along the x direction (SquareG).

The conformal array is constructed by conformal transformation of a regular hexagonal lattice situated in the complex plane:

$$z = n_1 b + n_2 b e^{i\pi/3} \tag{1}$$

where n_1 and n_2 are integers and b is a parameter. We apply a conformal transformation $w(z)$ given by

$$w = \frac{\pi}{2\alpha} + \frac{1}{i\alpha} \ln(i\alpha z) \tag{2}$$

where α is another parameter; this maps the points of the original lattice to the w plane. A semiannular section of the original lattice, specified by Im $z \geq 0$ and $r_{\rm in} \leq |z| \leq r_{\rm out}$, will be mapped to a rectangular region containing the conformal array. We take $r_{\rm out} = 36/\pi$, $\alpha = 1/r_{\rm out}$,

$r_{\rm in} = r_{\rm out}e^{-\pi/3}$, and $b^2 = (1 - e^{-2\pi/3}) \cdot (\sqrt{3}/\pi)$. This choice of parameters generates a conformal array in a 36×12 rectangular region, with approximately 1 lattice point per unit area.

The width of each pinning array segment is $a_p = 12\lambda$, and the segments are repeated three times across the sample as shown in Fig. 1. The total density of the pinning sites is $n_p = N_p/L^2 = 1.0$. The sample contains N_v vortices and we measure the magnetic field in units of B/B_ϕ, where B_ϕ is the matching field at which there is one vortex per pinning site. We obtain the initial vortex configuration by annealing from a high temperature molten state and cooling to $T = 0$ or to a low but finite fixed temperature. After annealing, we apply an ac driving force to all the vortices.

The dynamics of an individual vortex i is obtained by integrating the following overdamped equation of motion:

$$\eta \frac{d\mathbf{R}_i}{dt} = \mathbf{F}_i^{vv} + \mathbf{F}_i^{vp} + \mathbf{F}_i^{ac} + \mathbf{F}_i^{T} \ . \tag{3}$$

Here η is the damping constant which is set equal to 1. The repulsive vortex-vortex interaction force is given by $\mathbf{F}_i^{vv} = \sum_{j \neq i} F_0 K_1(R_{ij}/\lambda)\hat{\mathbf{R}}_{ij}$, where $\mathbf{R}_i$ is the location of vortex i, K_1 is the modified Bessel function, $R_{ij} = |\mathbf{R}_i - \mathbf{R}_j|$, $\hat{\mathbf{R}}_{ij} = (\mathbf{R}_i - \mathbf{R}_j)/R_{ij}$, $F_0 = \phi_0^2/(2\pi\mu_0\lambda^3)$, ϕ_0 is the flux quantum, and μ_0 is the permittivity. The vortex-pinning interaction force is $\mathbf{F}_i^{vp} = \sum_{k=1}^{N_p}(F_p R_{ik}^{(p)}/r_p)\Theta((r_p - R_{ik}^{(p)})/\lambda)\hat{\mathbf{R}}_{ik}^{(p)}$, where Θ is the Heaviside step function, $r_p = 0.25\lambda$ is the pinning radius, F_p is the pinning strength, $\mathbf{R}_k^{(p)}$ is the location of pinning site k, $R_{ik}^{(p)} = |\mathbf{R}_i - \mathbf{R}_k^{(p)}|$, and $\hat{\mathbf{R}}_{ik}^{(p)} = (\mathbf{R}_i - \mathbf{R}_k^{(p)})/R_{ik}^{(p)}$. All forces are measured in units of F_0 and lengths in units of λ. Thermal forces are represented by Langevin kicks $\mathbf{F}_i^T$ with the properties $\langle F_i^T(t)\rangle = 0$ and $\langle F_i^T(t)F_j^T(t')\rangle = 2\eta k_B T\delta_{ij}\delta(t-t')$, where k_B is the Boltzmann constant. The ac driving force is $\mathbf{F}_{ac} = F_{ac}\sin(\omega t)\hat{\mathbf{x}}$ where F_{ac} is the ac amplitude. To characterize the ratchet effect we measure the average net displacement of all vortices from their starting positions as a function of time, $\langle \Delta X\rangle = N_v^{-1}\sum_{i=1}^{N_v}(x_i(t) - x_i(t_0))$, where $x_i(t)$ is the x position of vortex i at time t and t_0 is an initial reference time. This measure produces a sinusoidal signal, as shown in Fig. 2; the presence of a net drift indicates that a ratchet effect is occurring. We condense this information into a single number $X_{\rm net}$, the value of $\langle \Delta X\rangle$ at $t - t_0 = 50$ ac drive cycles. Except where otherwise noted, we consider a fixed ac frequency of $\omega = 0.04$ and a time step of $\delta t = 0.02$, so that a single drive cycle has a period of 8000 simulation time steps.

III. RATCHET EFFECT

In Fig. 2 we plot the average net displacement $\langle \Delta X\rangle$ versus time for Conf, RandG, and SquareG arrays with $B/B_\phi = 1.0$, $F_p = 1.0$, and $F_{ac} = 0.55$ during 100 ac drive cycles. Here the overall drift of each curve indicates that all the arrays produce a ratchet effect with the vortices translating in the negative x direction. The Conf array generates the largest ratchet effect, with the vortices translating distances up to 2λ per drive cycle. The ratchet effect for the Conf array is about four times larger than that of the SquareG array and 20 times larger than that of the RandG array.

The relative effectiveness of the different arrays can be more clearly understood by plotting the trajectories of the vortices during the positive and negative portions of a single ac cycle. Figure 3(a,b) shows the trajectories for both halves of the ac cycle in a a RandG array with $B/B_\phi = 1.0$, $F_p = 1.5$ and $F_{ac} = 1.5$. Under both positive and negative drive, the vortices form disordered flow paths with a similar density that is independent of the driving direction. In contrast, in Fig. 3(c) during the positive portion of the ac driving cycle for the Conf array, almost no vortices can cross the densely pinned regions of the sample; instead, the vortices either become trapped at pining sites or remain localized in interstitial cages formed by the pinned vortices. Figure 3(d) shows that in the negative portion of the cycle for the Conf array, numerous vortices move into the interstitial regions and funnel through the conformal arch structures, producing significant vortex motion in the negative x direction. In the SquareG system, Figs. 3(e,f) show that vortex motion is strongly suppressed for both directions of drive and occurs only when interstitial vortices manage to squeeze between equally spaced occupied pinning sites. The barrier to this type of vortex motion is the same in each half of the cycle. In contrast, for the Conf array the perpendicular spacing between pinned vortices in the sparse portion of the array is larger than the equivalent spacing between pinned vortices in the dense portion of the array, so the interstitial vortices experience much different effective caging barriers when entering the sparse side of the array than when entering the dense side of the array. In the RandG arrays, channels of easy vortex flow occur somewhere in the sample with equal probability for both the positive and negative portions of the ac drive cycle.

In Fig. 4(a) we plot $X_{\rm net}$, the average net displacement per vortex after 50 ac drive cycles, versus F_p for Conf, RandG, and SquareG samples with $B/B_\phi = 1.0$ and $F_{ac} = 0.7$. For weak pinning $F_p < 0.7$, the vortices move elastically and easily slide over the pinning sites so that there is no ratchet effect in any of the arrays. For $F_p > 1.5$ most of the vortices become increasingly pinned and the ratchet effect is reduced. The optimal ratchet effect occurs for the Conf array at $F_p = 1.4$, where there is a mixture of pinned vortices coexisting with vortices that move temporarily through the interstitial regions as illustrated in Fig. 3(c,d). The SquareG array has a weaker ratchet effect in the range $0.8 < F_p < 1.4$, with a relatively sharp cutoff at the upper end of this range that occurs when the ability of the pinned vortices to shift inside the pinning sites is reduced, preventing the interstitial vortices from slipping between occupied pinning

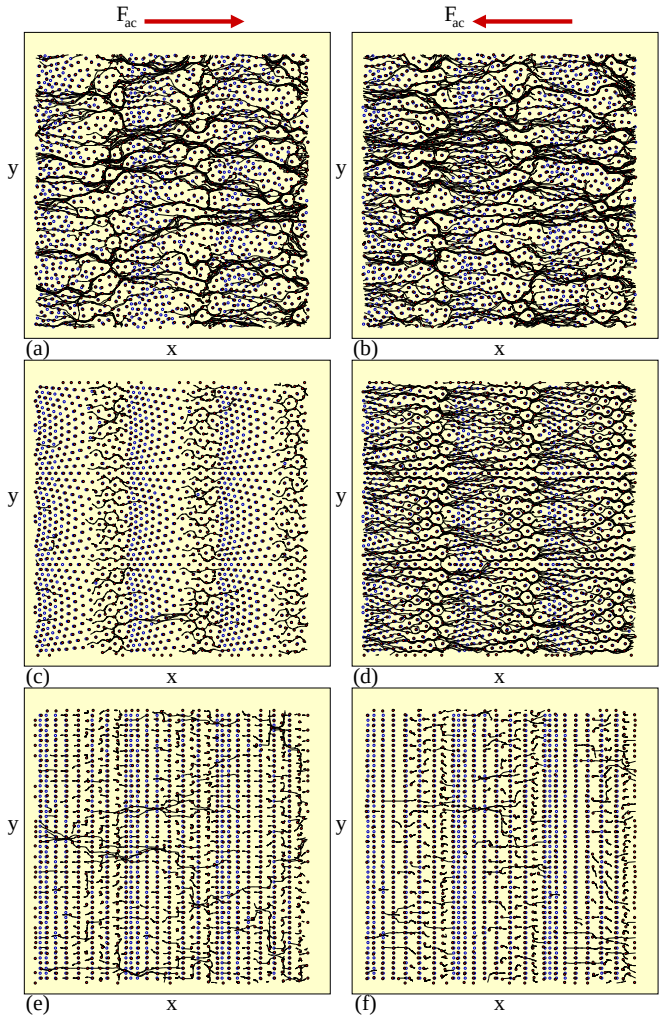

FIG. 3: The vortex locations (red dots), pinning site locations (open blue circles), and vortex trajectories (black lines) for samples with $B/B_\phi = 1.0$, $F_p = 1.5$, and $F_{ac} = 1.5$, highlighting the enhanced effectiveness of the ratchet mechanism in the Conf array. (a) The trajectories for the positive half of the ac drive cycle in the RandG array showing the formation of disordered flow channels. (b) The negative half of the ac drive cycle in the RandG array has a similar pattern and density of flow channels. (c) In the positive half of the ac drive cycle for the Conf array, the vortices cannot move past the densely pinned region. (d) In the negative half of the ac drive cycle in the Conf array, the vortices can easily funnel between the arches in the conformal array. (e) In the positive half of the ac drive cycle for the SquareG array, vortices can slip through the interstitial regions between pinned vortices. (f) Similar interstitial motion occurs in the negative half of the ac drive cycle for the SquareG array.

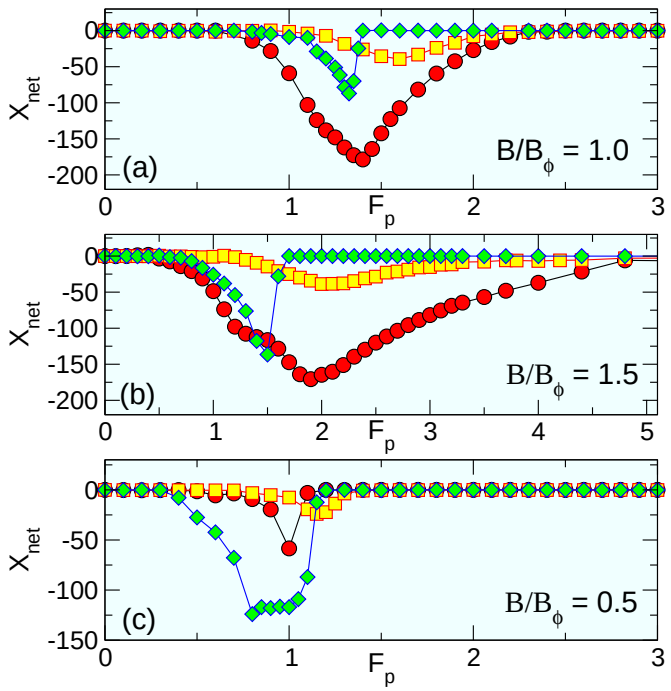

FIG. 4: $X_{\rm net}$, the average net displacement per vortex after 50 ac drive cycles, vs F_p for the Conf (red circles), RandG (yellow squares), and SquareG (green diamonds) arrays. Here $F_{ac} = 0.7$ and $n_p = 1.0$. In general, the ratchet effect is suppressed for weak pinning and for strong pinning. (a) At $B/B_\phi = 1.0$, the Conf array exhibits the strongest ratchet effects, followed by the SquareG array. The RandG array has the weakest ratchet effect. (b) At $B/B_\phi = 1.5$ the ratchet effect extends to higher values of F_p in all the systems. The Conf ratchet is still the most effective. (c) At $B/B_\phi = 0.5$, the SquareG ratchet is more effective than the Conf or RandG ratchets.

and causing the motion to become localized, as shown in Fig. 3(e,f). There is a weak ratchet effect for the RandG array with an extremum at $F_p = 1.6$ where the combination of the ac drive and the vortex-vortex interactions causes a portion of the vortices to depin. The maximum magnitude of the ratchet effect for the RandG array is smaller than that for the SquareG array; however, the effect occurs over a wider range of F_p. Figure 4(b) shows $X_{\rm net}$ versus F_p for $B/B_\phi = 1.5$, where there are more interstitial vortices. Here the range of F_p over which the ratchet effect occurs for the Conf and RandG arrays extends up to $F_p = 5.0$, with the ratcheting for $F_p > 2.1$ completely dominated by the flow of interstitial vortices. For the SquareG array the ratchet effect is lost for $F_p > 1.7$, the point at which the interstitial vortices can no longer slip through the one-dimensional interstitial channels of the array. In Fig. 4(c) we plot $X_{\rm net}$ versus F_p at $B/B_\phi = 0.5$, where there are few interstitial vortices. Here most of the motion occurs when vortices jump from one pinning site to another. The ratchet effect for all three arrays vanishes for $F_p > 1.4$ when vortex hopping is suppressed. At this vortex density, the ratchet effect is most pronounced for the SquareG array, where the vortices are able to hop along one-dimensional channels of pinning sites.

In Fig. 5(a) we plot $X_{\rm net}$ versus the ac drive amplitude F_{ac} for Conf, RandG, and SquareG samples with $F_p = 1.0$ and $B/B_\phi = 1.0$. For $F_{ac} < 0.35$, the vortices are

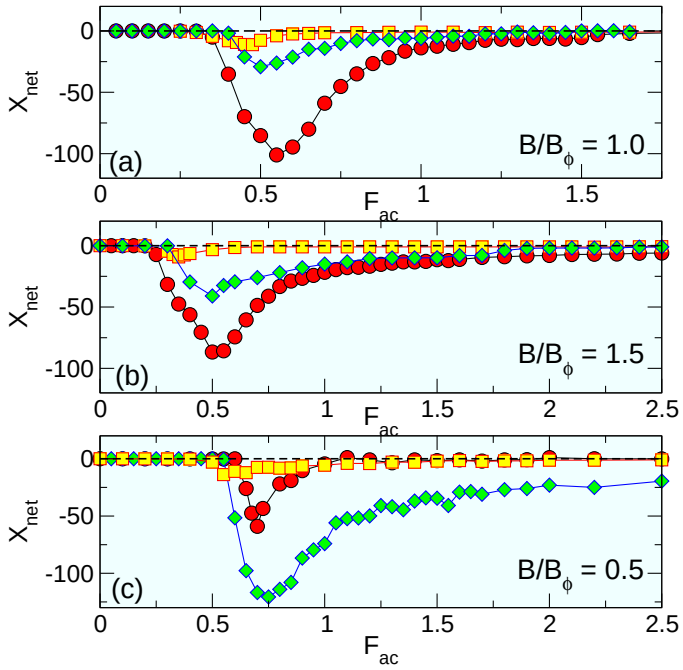

FIG. 5: $X_{\rm net}$ vs ac amplitude F_{ac} for Conf (red circles), RandG (yellow squares), and SquareG (green diamonds) arrays with $F_p = 1.0$ and $n_p = 1.0$. (a) At $B/B_\phi = 1.0$, the ratchet effect is reduced at low F_{ac} when the vortices are pinned as well as at higher F_{ac} when the vortices move rapidly over the pinning array. (b) $B/B_\phi = 1.5$. (c) At $B/B_\phi = 0.5$ the SquareG array produces the most effective ratchet.

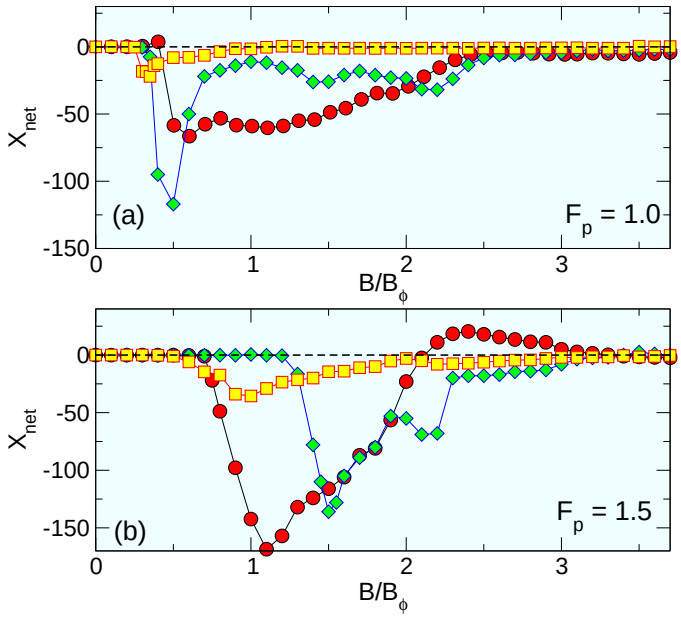

FIG. 6: $X_{\rm net}$ vs B/B_ϕ for Conf (red circles), RandG (yellow squares), and SquareG (green diamonds) arrays with $F_{ac} = 0.7$. (a) At $F_p = 1.0$ the ratchet effect is negative for the entire range of B/B_ϕ. (b) At $F_p = 1.5$ there is a reversal in the ratchet effect for the Conf array for $2.125 < B/B_\phi < 3.375$.

mostly pinned and the ratchet effect is absent for all three of the pinning geometries. At intermediate F_{ac} the Conf array has the strongest ratchet effect, with an extremum in $X_{\rm net}$ at $F_{ac} = 0.55$. The SquareG array has the next most effective ratchet effect, with an optimal magnitude at $F_{ac} = 0.5$. For higher values of F_{ac}, the vortices are all in motion during some portion of the driving cycle and the ratchet effect gradually decreases to zero with increasing F_{ac}. We observe a similar trend at $B/B_\phi = 1.5$ as shown in Fig. 5(b). Here the ratchet effect for the Conf array extends up to much larger values of F_{ac}; however, the maximum value of $|X_{\rm net}|$ is slightly smaller than for the $B/B_\phi = 1.0$ case. For $B/B_\phi = 0.5$ in Fig. 5(c), the dominant motion is hopping of vortices from pinning site to pinning site. Here the ratchet effect is strongest for the SquareG array, similar to what is shown in Fig. 4(c).

IV. RATCHET REVERSAL

In Fig. 6(a) we plot $X_{\rm net}$ versus B/B_ϕ for Conf, RandG, and SquareG arrays with $F_p = 1.0$ and $F_{ac} = 0.7$. Here the Conf array outperforms the RandG array for all fields and the SquareG array for $0.6 < B/B_\phi < 2.0$. For $B/B_\phi > 2.0$ the vortex-vortex interactions become dominant and the ratchet effect is suppressed in all the arrays. In the SquareG array, due to the periodic ordering along the y direction, some commensuration effects occur, such as enhanced pinning near $B/B_\phi = 1.0$ which locally suppresses the ratchet effect.

Figure 6(b) shows $X_{\rm net}$ versus B/B_ϕ for $F_p = 1.5$. In this case, the ratchet effect for the SquareG array is lost for $B/B_\phi < 1.2$ when the vortices become strongly pinned at the pinning sites. In general, the ratchet effect for the Conf array is stronger than that for the SquareG and RandG arrays, with a local extremum for the ratchet effect in the negative or normal direction occurring at $B/B_\phi = 1.05$. The SquareG array has a local extremum in $X_{\rm net}$ in the negative direction at $B/B_\phi = 1.5$, followed by a sharp drop in $X_{\rm net}$ for $B/B_\phi > 2.25$. We find a ratchet reversal in the Conf array, where $X_{\rm net}$ switches from negative to positive over the range $2.1 < B/B_\phi < 3.375$. There is a local maximum in the positive ratchet effect at $B/B_\phi = 2.4$. In Fig. 7(a) we show a highlight of $X_{\rm net}$ versus B/B_ϕ from Fig. 6(b) for the Conf array indicating that two reversals in the ratchet effect occur. Figure 7(b) illustrates $\langle \Delta X \rangle$ vs time in ac drive cycles for the system in Fig. 7(a) at $B/B_\phi = 1.9$, where the motion is in the negative x direction, and at $B/B_\phi = 2.4$, where the motion is in the positive x direction, showing more clearly the change in the net direction of vortex motion.

In Fig. 8(a) we plot $X_{\rm net}$ versus F_{ac} for a Conf array with $F_p = 1.5$ at $B/B_\phi = 2.4$, where there are multiple reversals in the ratchet effect. For $F_{ac} < 0.1$ there is no ratchet effect since the vortices move only small distances. A negative ratchet effect occurs for $0.1 < F_{ac} < 0.45$, while for $0.45 \leq F_{ac} < 1.3$ there is a positive ratchet effect with a maximum amplitude at

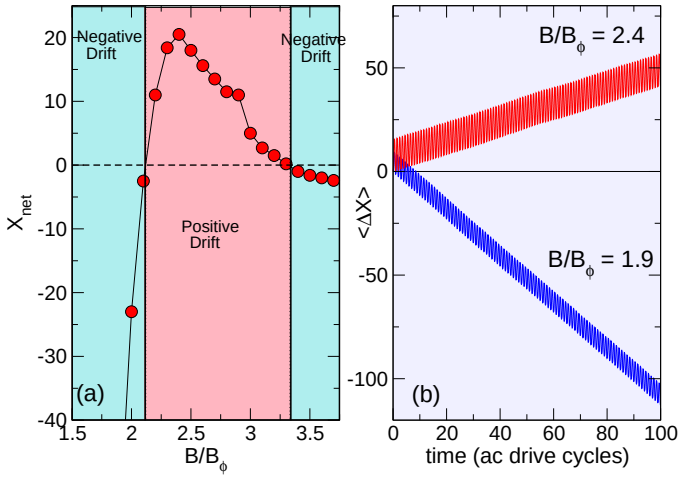

FIG. 7: (a) $X_{\rm net}$ vs B/B_ϕ for the Conf array in Fig. 6(b) highlighting the vortex ratchet reversal effect from negative for $B/B_\phi < 2.25$ to positive for $2.25 < B/B_\phi < 3.375$ to negative again at higher fields. (b) $\langle \Delta X \rangle$ vs time in ac drive cycle numbers for the system in (a) at $B/B_\phi = 1.9$ (lower blue curve) where the vortex motion is in the negative x direction and at $B/B_\phi = 2.4$ (upper red curve) where the motion is in the positive x direction.

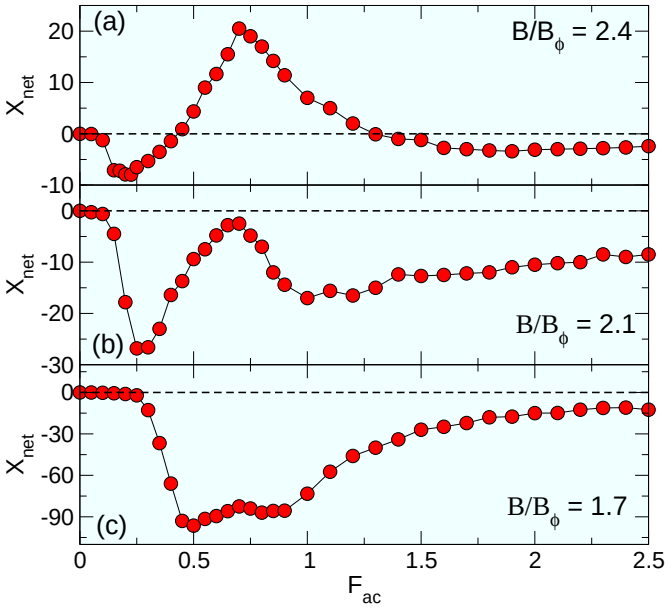

FIG. 8: $X_{\rm net}$ vs F_{ac} for Conf arrays with $F_p = 1.5$. (a) At $B/B_\phi = 2.4$, there is a transition from a negative ratchet effect at low F_{ac} to a positive ratchet effect, followed by a second transition back to a negative ratchet effect. (b) At $B/B_\phi = 2.1$ the ratchet effect is always negative; however, there is a local minimum and a local maximum of the ratchet effect. (c) At $B/B_\phi = 1.7$, the ratchet effect is always negative and has few features.

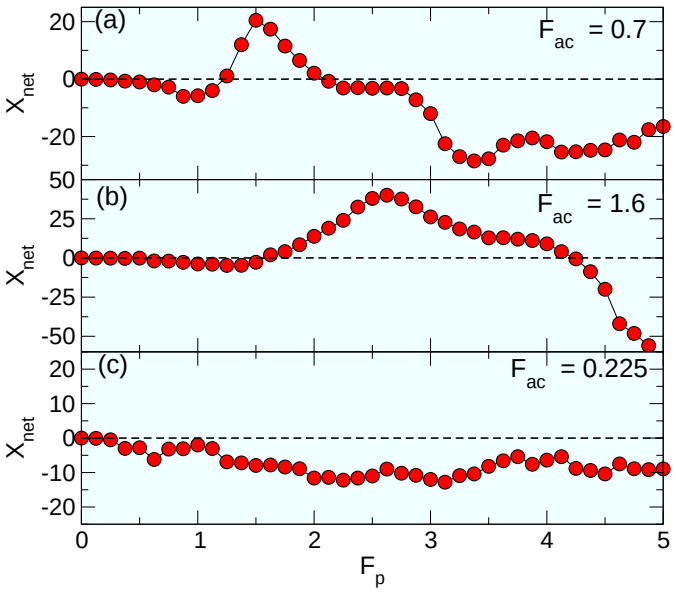

FIG. 9: $X_{\rm net}$ vs F_p for Conf arrays with $B/B_\phi = 2.4$. (a) At $F_{ac} = 0.7$ there are multiple reversals as F_p increases. (b) At $F_{ac} = 1.6$ there are again multiple reversals and the positive ratchet effect extends over a wider range of F_p. (c) At $F_{ac} = 0.225$ there is a weak negative ratchet effect.

$F_{ac} = 0.7$. There is another transition to a weaker negative ratchet effect for $F_{ac} > 0.13$, and $X_{\rm net}$ gradually approaches zero for high values of F_{ac}. Figure 8(b) shows that at $B/B_\phi = 2.1$, the ratchet effect is always negative; however, there are still local features in the response such as at $0.3 < F_{ac} < 1.0$ where the negative ratchet effect is strongly reduced. In Fig. 8(c) at $B/B_\phi = 1.7$, the ratchet effect is strongly negative with an extremum in $X_{\rm net}$ near $F_{ac} = 0.5$. The ratchet effect goes to zero for increasing F_{ac}.

In Fig. 9(a) we show $X_{\rm net}$ versus F_p for a Conf array at $B/B_\phi = 2.4$ and $F_{ac} = 0.7$. There is a negative ratchet effect for $0 < F_p < 1.25$, a positive ratchet effect for $1.25 \leq F_p < 2.1$, and a much larger negative ratchet effect for $F_p > 3.0$. At intermediate F_p when there is a positive ratchet effect, vortices can be temporarily trapped by pinning sites. The negative ratchet effect for large F_p arises from the interstitial flow of vortices, and $X_{\rm net}$ saturates at large F_p since the caging barrier experienced by interstitial vortices from the neighboring pinned vortices does not increase with increasing F_p. In Fig. 9(b), at $F_{ac} = 1.6$ there is a negative ratchet effect for $0 < F_p < 1.625$, a positive ratchet effect for $1.625 \leq F_p < 4.25$, and another negative ratchet regime for $F_p > 4.25$. The vortices at the pinning sites remain permanently pinned for $F_p > 4.25$. The positive ratchet effect is larger and extends out to higher values of F_p for the $F_{ac} = 1.6$ system compared to the $F_{ac} = 0.7$ system. Figure 9(c) shows that at $F_{ac} = 0.225$, there is a weak negative ratchet effect for all values of F_p. Although we focus here on the Conf array, we also found that some

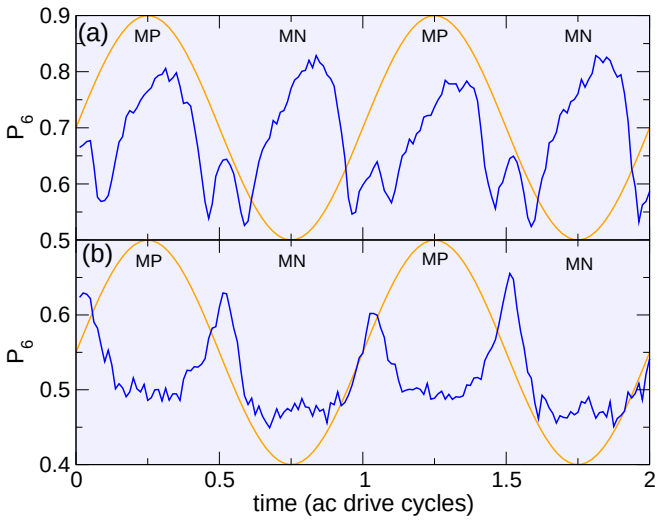

FIG. 10: Dark blue lines: P_6, the fraction of sixfold-coordinated particles, vs time in ac drive cycles for Conf arrays from Fig. 9(a) with $B/B_\phi = 2.4$ and $F_{ac} = 0.7$. Light orange lines indicate the phase of the drive cycle. MP is the maximum positive drive and MN is the maximum negative drive. (a) At $F_p = 0.875$ the ratchet effect is negative. The system is most ordered whenever the magnitude of the ac drive is maximum; however, the ordering peaks for the negative portions of the drive cycle are slightly higher than those for the positive portions of the drive cycle. (b) At $F_p = 1.5$ the ratchet effect is positive. The system is most ordered whenever the magnitude of the ac drive is close to zero, but the net motion is determined by the relatively larger ordering at MP points compared to MN points.

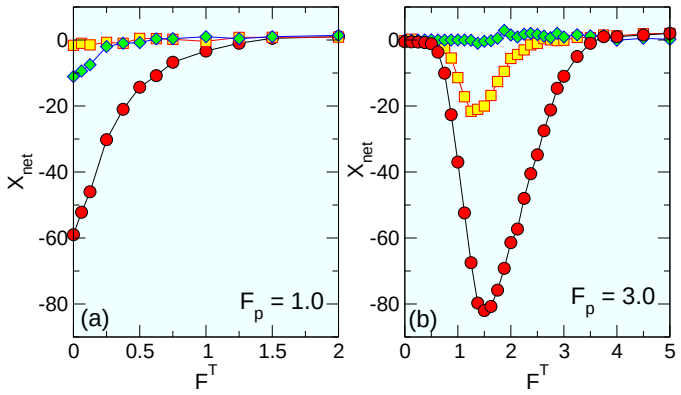

FIG. 11: $X_{\rm net}$ vs F^T for Conf (red circles), RandG (yellow squares), and SquareG (green diamonds) arrays with $B/B_\phi = 1.0$ and $F_{ac} = 0.7$. (a) At $F_p = 1.0$, thermal effects reduce the ratchet effect. (b) At $F_p = 3.0$ thermal effects can increase the ratchet effect over a range of F^T.

weak ratchet reversals are possible in the SquareG array; however, we did not observe a vortex ratchet reversal for the RandG array.

In order to better understand the vortex dynamics and ordering during an individual ac cycle, in Fig. 10 we plot the time series of the fraction of sixfold-coordinated vortices, $P_6 = N_v^{-1} \sum_{i=1}^{N_v} \delta(z_i - 6)$, versus time. Here z_i, the coordination number of vortex i, is obtained from a Voronoi construction. Superimposed over the plot is a curve showing the phase of the ac drive, and the points at which the drive reaches its maximum positive value are marked MP while those at which the drive reaches its maximum negative value are marked MN. Figure 10(a) shows P_6 versus time for the system from Fig. 9(a) with $B/B_\phi = 2.4$ and $F_{ac} = 0.7$ at $F_p = 0.875$ where there is a negative ratchet effect. Here $P_6 = 0.65$ at the start of each drive cycle when the drive magnitude is zero, deceases slightly when the drive becomes positive and the system disorders, then reaches its highest values of $P_6 \approx 0.8$ in the MP portions of the drive cycle and $P_6 \approx 0.83$ in the MN portions of the drive cycle. When the magnitude of the ac drive is maximum, all the vortices move elastically, and since they are slightly more ordered during the negative cycle of the drive, they can slide slightly further in the negative x direction than in the positive x direction, giving a negative ratchet effect. At $F_p = 1.5$ in Fig. 10(b), the ratchet effect is positive and the vortex ordering is reversed. The vortices are now the most ordered when the magnitude of the ac drive is close to zero, and they are disordered when the ac drive magnitude reaches a maximum. During the MP portion of the drive cycle, $P_6 = 0.5$, while in the MN portion of the drive cycle the system is more disordered with $P_6 = 0.47$. The more ordered vortices are able to slide slightly further in the positive x direction, resulting in a net positive ratchet effect. There is also an asymmetry in the ordering at the zero force portions of the drive cycle. The value of P_6 at cycle times of 0.0 and 1.0 is smaller than that at times of 0.5 and 1.5; however, since the vortices are not moving during this portion of the cycle, this asymmetry does not produce a preferred direction of motion. In general we find that the ordering of the vortices at the MP and MN points of the drive determines the direction of the ratchet motion, with the net ratchet effect occurring in whichever drive direction generates the most ordered vortex arrangement.

V. THERMAL EFFECTS

We next consider thermal effects on the ratchet response. For weak pinning, the addition of thermal fluctuations monotonically decreases the ratchet effect for all three geometries, as shown in Fig. 11(a) for $F_p = 1.0$, $F_{ac} = 0.7$, and $B/B_\phi = 1.0$. As before, the ratchet effect is most pronounced for the conformal array. As F_p increases, the vortices become more strongly pinned, and the addition of thermal fluctuations can increase the ratchet effect by permitting vortices to escape from pinning sites or interstitial caging sites via thermal activation. In Fig. 11(b) we plot $X_{\rm net}$ versus F^T in samples with F_p increased to $F_p = 3.0$, showing a strong ratchet

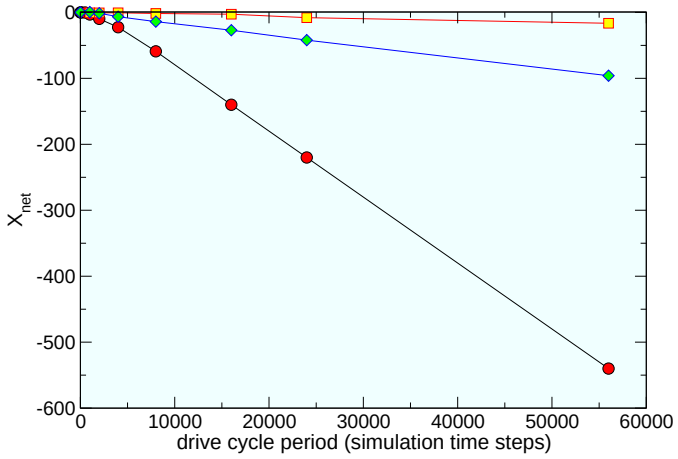

FIG. 12: $X_{\rm net}$ versus ac cycle period in simulation time steps for Conf (red circles), RandG (yellow squares), and SquareG (green diamonds) arrays with $B/B_\phi = 1.0$, $F_{ac} = 0.7$, and $F_p = 1.0$. $X_{\rm net}$ increases linearly with the drive cycle period.

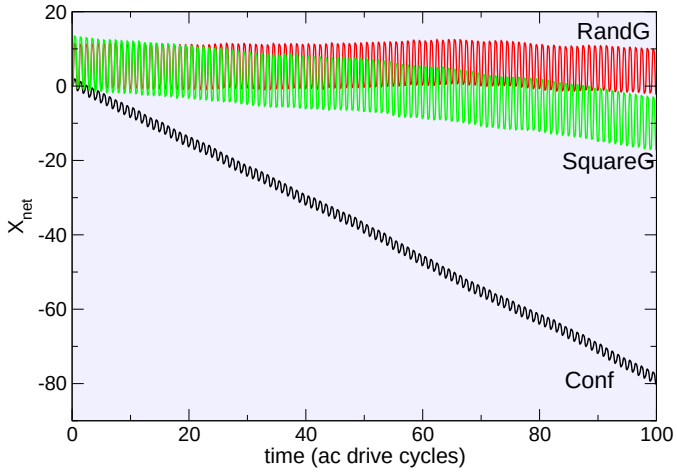

FIG. 13: $\langle \Delta X \rangle$ vs time measured in ac drive cycles for colloidal particles interacting with a Conf array (bottom black curve), a SquareG array (middle green curve), and a RandG array (upper red curve) with $N_c/N_p = 1.0$, $F_p = 1.0$, $F_{ac} = 0.55$, and $A_c = 0.01$. As in the vortex case shown in Fig. 2, the Conf array produces the strongest ratchet effect.

effect in the Conf array. Here, the ratchet effect is lost at small F^T since the vortices are strongly pinned, and the ratchet effect also disappears for high values of F^T when the thermal fluctuations become so strong that the vortices enter a molten state that interacts too weakly with the substrate for an asymmetry in the response to positive and negative drives to be noticeable. The largest ratchet signatures appear for intermediate F^T. In general, when F_p increases, the point at which the magnitude of the ratchet effect is largest shifts to higher values of F^T.

We find that $X_{\rm net}$ increases linearly as the period of the ac driving cycle increases, as illustrated in Fig. 12 for Conf, RandG, and SquareG arrays with $B/B_\phi = 1.0$, $F_p = 1.0$, and $F_{ac} = 0.7$. As the other parameters are varied, we find a robust increase in the magnitude of the ratchet effect with decreasing ac frequency.

VI. RATCHET EFFECTS FOR COLLOIDAL PARTICLES

Ratchet effects can be generated in systems of colloidal particles interacting with various types of periodic arrays of traps that are created using optical means[51–54]. The ability to make structures similar to conformal lattices has been demonstrated by Xiao *et al.*[55], who examined a colloidal ratchet effect on optical traps forming Fibonacci spirals. In that case the ratchet effect is induced by rotating the potential through a three-step cycle. Here we consider the ac-driven motion of colloidal particles over a Conf array. The equation of motion for colloids is similar to that given in Eqn. 1 for vortices, except that the pairwise repulsive colloid-colloid interaction potential has the form $V(R_{ij}) = A_c \exp(-\kappa R_{ij})/R_{ij}$, where $E_0 = q^2 Z^{*2}/4\pi\epsilon\epsilon_0 a_0$, q is the dimensionless interaction strength, Z^* is the effective charge of the colloidal particles, ϵ is the solvent dielectric constant, and $1/\kappa$ is the screening length which we set equal to 1.0. The number of colloids in the sample is N_c. For our parameters, the interactions between colloids for $R_{ij} < 1$ is much larger than the interactions between vortices separated by the same distance, while for $R_{ij} > 1$ the colloidal interaction strength falls off much more rapidly than the vortex-vortex interaction strength, so that nearest neighbor interactions are dominant in the colloidal system. We have conduced a series of simulations for colloidal particles moving through Conf, RandG, and SquareG pinning landscapes under an ac driving force, and find results very similar to those obtained in the vortex system. For example, in Fig. 13 we plot $\langle \Delta X \rangle$ versus time for colloids interacting with Conf, SquareG, and RandG arrays for $N_c/N_p = 1.0$, $F_p = 1.0$, $F_{ac} = 0.55$, and $A_c = 0.01$, where we observe that just as in the vortex case, the Conf array produces the most pronounced ratchet effect, the SquareG array shows a weak ratchet effect, and the RandG array does not exhibit a ratchet effect. Since the effective charge on the colloids can be changed experimentally, it is possible to hold the substrate strength fixed and modify how strongly the colloids interact with one another. In Fig. 14(a) we plot $X_{\rm net}$ versus A_c for the Conf array from Fig. 13, and in Fig. 14(b) we show the corresponding fraction of sixfold coordinated colloids P_6 versus A_c. For $A_c = 0$ the colloids all become pinned in the pinning sites since $F_{ac} < F_p$. As A_c increases, the colloid-colloid interactions become important and a ratchet effect arises with a maximum amplitude near $A_c = 1.0$. The largest ratchet effect is associated with a sixfold ordering fraction of $P_6 = 0.6$, indicating that the colloids are still disordered, with some colloids trapped

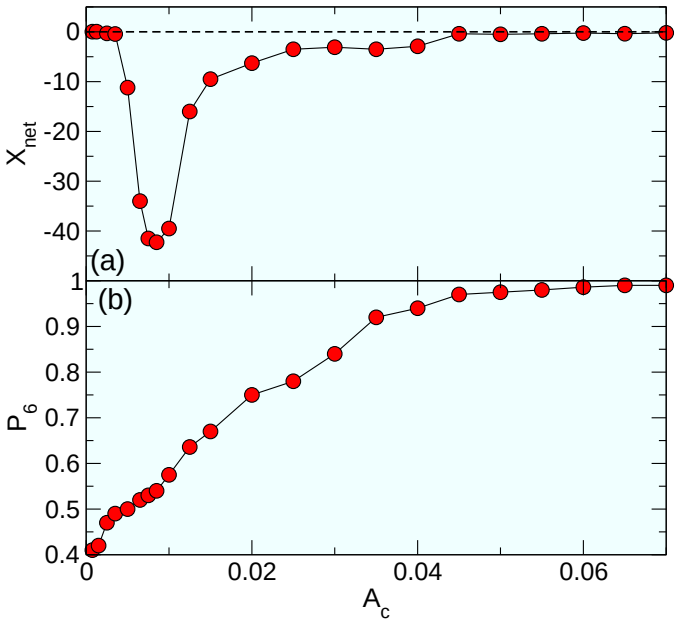

FIG. 14: (a) $X_{\rm net}$ vs colloid-colloid interaction strength A_c for the Conf colloid system in Fig. 13 with $N_c/N_p = 1.0$, $F_p = 1.0$, and $F_{ac} = 0.55$. (b) The corresponding fraction of sixfold coordinated colloids P_6 vs A_c. Here the maximum ratchet effect occurs when $P_6 = 0.6$, indicating that although colloid-colloid interactions remain important, the system is in a disordered state. When the system forms a crystalline state with $P_6 \approx 1.0$, the ratchet effect disappears.

in pinning sites and others occupying interstitial regions between pins. For $A_c > 0.01$ the ratchet effect begins to diminish with increasing A_c while simultaneously P_6 increases, indicating an increase in the ordering of the colloids. For $A_c > 0.04$, the colloids form a rigid triangular lattice as indicated by the fact that $P_6 \approx 1.0$, and the ratchet effect disappears. These results show that in order for a ratchet effect to appear in the gradient pinning arrangements, it is generally necessary for plasticity or defects in the colloid or vortex lattice to appear. Our results with the colloidal system indicate that pronounced ratchet effects should be realizable in a variety of systems where assemblies of interacting particles are driven with an ac drive over conformal array substrates.

VII. SUMMARY

We have examined ratchet effects for ac driven vortices interacting with a conformal pinning array, square gradient array, and a random arrangement of pinning sites containing a gradient along one direction. We find that in general the conformal pinning array produces the most pronounced ratchet effect, especially for fields larger than the first matching field. The ratchet effect in the conformal array is enhanced due to the fact that the pinning sites in the low density regions of the substrate are more widely spaced in the direction perpendicular to the net gradient in the pinning, allowing an easy flow of interstitial vortices along the gradient direction. In contrast, in the square gradient array, there is no variation in the perpendicular distance between the pinning sites throughout the array, so that the barrier to interstitial vortex motion is the same for both directions of drive. As a result, the ratchet effect in this array is reduced when interstitial vortices are present. There are large channels of vortex flow in the random gradient array that form for either direction of drive, minimizing the ratchet effect. We also observe a series of vortex ratchet reversals in the conformal pinning array as a function of ac drive amplitude, vortex density, and pinning strength. The amount of order present in the vortex lattice during different phases of the ac driving cycle determines the direction of the ratchet effect. Finally, we consider colloidal particles driven over the same types of arrays, and find that in this case the ratchet effect for the conformal array is also larger than that in the square gradient array or the random gradient array, suggesting that pronounced ratchet effects should be a general feature of particles driven over conformal arrays.

Acknowledgments

This work was carried out under the auspices of the NNSA of the U.S. DoE at LANL under Contract No. DE-AC52-06NA25396.

[1] P. Reimann, Phys. Rep. **361**, 57 (2002).
[2] P. Hänggi and F. Marchesoni, Rev. Mod. Phys. **81**, 387 (2009).
[3] J. Rousselet, L. Salome, A. Ajdari, and J. Prost, Nature (London) **370**, 446 (1994).
[4] A. Libál, C. Reichhardt, B. Jankó, and C. J. Olson Reichhardt, Phys. Rev. Lett. **96**, 188301 (2006).
[5] R.L. Smith, G.C. Spalding, K. Dholakia, and M.P. MacDonald, J. Optics A **9**, S134 (2007).
[6] Z. Farkas, P. Tegzes, A. Vukics, and T. Vicsek, Phys. Rev. E **60**, 7022 (1999).
[7] J. F. Wambaugh, C. Reichhardt, and C. J. Olson, Phys. Rev. E **65**, 031308 (2002).
[8] J. Bader, R.W. Hammond, S.A. Henck, M.W. Deem, G.A. McDermott, J.M. Bustillo, J.W. Simpson, G.T. Mulhern, and J.M. Rothberg, Proc. Natl. Acad. Sci. (USA) **96**, 13165 (1999).
[9] M.T. Downton, M.J. Zuckermann, E.M. Craig, M. Plischke, and H. Linke, Phys. Rev. E **73**, 011909 (2006).
[10] C.S. Lee, B. Jankó, I. Derényi, and A. L. Barabási, Nature

(London) **400**, 337 (1999).
[11] J.F. Wambaugh, C. Reichhardt, C.J. Olson, F. Marchesoni, and F. Nori, Phys. Rev. Lett. **83**, 5106 (1999).
[12] C.J. Olson, C. Reichhardt, B. Jankó, and F. Nori, Phys. Rev. Lett. **87**, 177002 (2001).
[13] J.E. Villegas, S. Savelev, F. Nori, E.M. Gonzalez, J.V. Anguita, R. Garcia, and J.L. Vicent, Science **302**, 1188 (2003).
[14] C.C. de Souza Silva, J. Van de Vondel, M. Morelle, and V.V. Moshchalkov, Nature (London) **440**, 651 (2006).
[15] B.L.T. Plourde, IEEE Trans. Appl. Supercond. **19**, 3698 (2009).
[16] Q. Lu, C. Reichhardt, and C. Reichhardt, Phys. Rev. B **75**, 054502 (2007).
[17] V.A. Shklovskij and O.V. Dobrovolskiy, Phys. Rev. B **84**, 054515 (2011).
[18] V.A. Shklovskij, V.V. Sosedkin, and O.V. Dobrovolskiy, J. Phys.: Condens. Matter **26**, 025703 (2014).
[19] V.A. Shklovskij and V.V. Sosedkin, Phys. Rev. B **80**, 214526 (2009).
[20] K. Yu, T.W. Heitmann, C. Song, M.P. DeFeo, B.L.T. Plourde, M.B.S. Hesselberth, and P.H. Kes, Phys. Rev. B **76**, 220507(R) (2007).
[21] C. J. Olson Reichhardt and C. Reichhardt, Phys. Rev. B **81**, 224516 (2010).
[22] N.S. Lin, T.W. Heitmann, K. Yu, B.L.T. Plourde, and V.R. Misko, Phys. Rev. B **84**, 144511 (2011).
[23] G. Karapetrov, V. Yefremenko, G. Mihajlović, J.E. Pearson, M. Iavarone, V. Novosad, and S.D. Bader, Phys. Rev. B **86**, 054524 (2012).
[24] V. Vlasko-Vlasov, T. Benseman, U. Welp, and W.K. Kwok, Supercond. Sci. Technol. **26**, 075023 (2013).
[25] D. Cerbu, V.N. Gladilin, J. Cuppens, J. Fritzsche, J. Tempere, J.T. Devreese, V.V. Moshchalkov, A.V. Silhanek, and J. Van de Vondel, New J. Phys. **15**, 063022 (2013).
[26] B.Y. Zhu, F. Marchesoni, V.V. Moshchalkov, and F. Nori, Phys. Rev. B **68**, 014514 (2003).
[27] J. Van de Vondel, C.C. de Souza Silva, B.Y. Zhu, M. Morelle, and V.V. Moshchalkov, Phys. Rev. Lett. **94**, 057003 (2005).
[28] C.C. de Souza Silva, J. Van de Vondel, B.Y. Zhu, M. Morelle, and V.V. Moshchalkov, Phys. Rev. B **73**, 014507 (2006).
[29] C.J. Olson Reichhardt and C. Reichhardt, Physica C **432**, 125 (2005).
[30] J. Van de Vondel, V.N. Gladilin, A.V. Silhanek, W. Gillijns, J. Tempere, J.T. Devreese, and V.V. Moshchalkov, Phys. Rev. Lett. **106**, 137003 (2011).
[31] D. Perez de Lara, M. Erekhinsky, E.M. Gonzalez, Y.J. Rosen, I.K. Schuller, and J.L. Vicent, Phys. Rev. B **83**, 174507 (2011).
[32] L. Dinis, E.M. González, J.V. Anguita, J.M.R. Parrondo, and J.L. Vicent, Phys. Rev. B **76**, 212507 (2007).
[33] L. Dinis, E.M. González, J.V. Anguita, J.M.R. Parrondo, and J.L. Vicent, New J. Phys. **9**, 366 (2007).
[34] D. Perez de Lara, F.J. Castaño, B.G. Ng, H.S. Korner, R.K. Dumas, E.M. Gonzalez, K. Liu, C.A. Ross, I.K. Schuller, and J.L. Vicent, Phys. Rev. B **80**, 224510 (2009).
[35] A. Palau, C. Monton, V. Rouco, X. Obradors, and T. Puig, Phys. Rev. B **85**, 012502 (2012).
[36] W. Gillijns, A.V. Silhanek, V.V. Moshchalkov, C.J. Olson Reichhardt, and C. Reichhardt, Phys. Rev. Lett. **99**, 247002 (2007).
[37] T.C. Wu, R. Cao, T.J. Yang, L. Horng, J.C. Wu, and J. Kolacek, Solid State Commun. **150**, 280 (2010).
[38] T.C. Wu, L. Horng, J.C. Wu, R. Cao, J. Kolacek, and T.J. Yang, J. Appl. Phys. **102**, 033918 (2007).
[39] D. Ray, C.J. Olson Reichhardt, B. Jankó, and C. Reichhardt, Phys. Rev. Lett. **110**, 267001 (2013).
[40] D. Ray, C. Reichhardt, C.J. Olson Reichhardt, and B. Jankó, Physica C **503**, 123 (2014).
[41] D. Ray, C. Reichhardt, and C. J. Olson Reichhardt, Phys. Rev. B **90**, 094502 (2014).
[42] P. Pieranski, in *Phase Transitions in Soft Condensed Matter*, edited by T. Riste and D. Sherrington (Plenum, New York, 1989), p. 45; F. Rothen, P. Pieranski, N. Rivier, and A. Joyet, Eur. J. Phys. **14**, 227 (1993).
[43] F. Rothen and P. Pieranski, Phys. Rev. E **53**, 2828 (1996).
[44] M. Mancini and C. Oguey, Eur. Phys. J. E **17**, 119 (2005).
[45] A. Mughal and D. Weaire, Proc. Royal Soc. A **465**, 219 (2009).
[46] A. Mughal and M.A. Moore, Phys. Rev. E **76**, 011606 (2007).
[47] Y.L. Wang, M.L. Latimer, Z.L. Xiao, R. Divan, L.E. Ocola, G.W. Crabtree, and W.K. Kwok, Phys. Rev. B **87**, 220501(R) (2013).
[48] S. Guénon, Y.J. Rosen, A.C. Basaran, and I.K. Schuller, Appl. Phys. Lett. **102**, 252602 (2013).
[49] M. Motta, F. Colauto, W.A. Ortiz, J. Fritzsche, J. Cuppens, W. Gillijns, V.V. Moshchalkov, T.H. Johansen, A. Sanchez, and A.V. Silhanek, Appl. Phys. Lett. **102**, 212601 (2013).
[50] V.R. Misko and F. Nori, Phys. Rev. B **85**, 184506 (2012).
[51] P. T. Korda, G. C. Spalding, and D. G. Grier, Phys. Rev. B **66**, 024504 (2002).
[52] C. Reichhardt and C. J. Olson, Phys. Rev. Lett. **88**, 248301 (2002).
[53] M. Brunner and C. Bechinger, Phys. Rev. Lett. **88**, 248302 (2002).
[54] J. Mikhael, J. Roth, L. Helden, and C. Bechinger, Nature (London) **454**, 501 (2008).
[55] K. Xiao, Y. Roichman, and D.G. Grier, Phys. Rev. E **84**, 011131 (2011).